NASA Technical Paper 3538

September 1995

An X–Band Mixer Engineered for 77–K Operation

Robert R. Romanofsky

National Aeronautics and Space Administration

NASA
Technical
Paper
3538

1995

An X–Band Mixer Engineered for 77–K Operation

Robert R. Romanofsky
Lewis Research Center
Cleveland, Ohio

National Aeronautics and
Space Administration
Office of Management
Scientific and Technical
Information Program
1995

An X–Band Mixer Engineered for 77–K Operation

Robert R. Romanofsky
National Aeronautics and Space Administration
Lewis Research Center
Cleveland, Ohio 44135

Summary

An X-band Si-diode singly balanced mixer developed specifically for cryogenic operation is presented. In order to reduce thermal demands on a mechanical cooler, the mixer was designed to operate with a minimum of local oscillator (LO) power. That is, since the LO had to be cooled to reduce phase noise, it was desirable to minimize the LO drive. Novel embedding circuit strategy was responsible for nearly theoretical performance. The signal-matching circuit simultaneously provided a reactive termination to the image, sum, and first, second, and third LO harmonic frequencies. A conversion loss of 3.2 dB at 77 K with an LO drive of +1 dBm was measured. This loss included IF filter, dc block, and hybrid coupler losses. Mixer conversion loss is shown to be consistent with the theoretical performance limit expected from the intrinsic diode. The relationship among junction capacitance, flat-band potential, and conversion loss is examined.

Introduction

The benefit of cryogenic cooling to low noise receiver components is well known. For example, the noise temperature of high electron mobility transistor (HEMT) amplifiers was reduced by as much as a factor of eight by lowering the physical temperature of the device from 300 K to below 20 K from X- through Ka-band (refs. 1 and 2). Concomitantly the gain increased by a factor of two to four. Similar cooling of a Schottky barrier diode mixer (refs. 3 and 4) also reduced the mixer's shot noise by at least a factor of two in the microwave through millimeter-wave range.

This paper describes a narrow bandwidth mixer designed specifically for operation near 77 K. The mixer was originally developed as part of a miniaturized hybrid semiconductor-superconductor X-band downconverter. It was under investigation by the NASA Lewis Research Center and the Jet Propulsion Laboratory for potential deep space and commercial communications applications (ref. 5). The nominal input frequency was 7.1 to 7.25 GHz, and the output frequency was 1.15 to 1.3 GHz. From practical cooling and optimal performance perspectives, 77 K is a desirable operating temperature on which to compromise. Most of the benefits of device- and circuit-cooling have already been realized, and space-qualified coolers are available to manage thermal loads of at least several hundred milliwatts.

Demands on the mixer were twofold. First, to optimize receiver sensitivity since front-end gain was limited, the mixer was required not only to downconvert the signal without adversely affecting the pre-amplifier but also to minimize the signal degradation. Hence, low conversion loss, a low noise figure, and a high port-to-port isolation were desirable. Second, the mixer had to minimize thermal demands on the cooler by operating with a starved local oscillator (LO). Because the LO was inherently inefficient and had to be cooled in order to reduce phase noise, minimizing the required drive level of the mixer was tantamount to reducing the cooling power requirement. For example, if the LO is stabilized with a superconducting resonator and has an efficiency of 10 percent and if the mixer requires 10 dBm of LO drive, then the cryocooler heat load capacity must be increased by about 100 mW. Cooling the mixer increases the overall receiver sensitivity and permits convenient integration of all the critical front-end functions. Many conventional mixers with competing performance would severely tax the cooler. Figure 1 shows the conversion loss performance of a very good commercially available mixer (Watkins-Johnson WJ-M80LC), without provision for bias, as a function of temperature.

The design reported herein incorporates partial enhancement by using the low-pass matching circuit and quarter-wave radial stubs to reject the sum frequency ($f_{RF} + f_{LO}$) and the second and third LO harmonics. The impedance, as seen by each diode at the image frequency, approaches an open circuit.

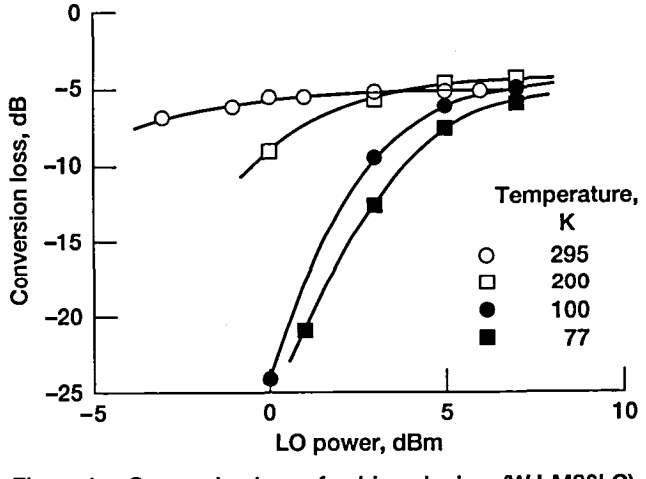

Figure 1.—Conversion loss of unbiased mixer (WJ-M80LC) as a function of LO power, with operating temperature as a parameter.

This report shows that through accurate device modeling, conversion loss can be optimized for cryogenic operation and perform significantly better than at room temperature, evidently by exploiting the increased nonlinearity of the cooled diode. This experimental evidence also complements recent work (refs. 6 and 7) which claims that optimal performance is achieved only if the instantaneous diode current exceeds the flatband current for part of the LO cycle. Experimental data on the behavior of junction capacitance are also presented and compared to theoretical behavior. The relationship of junction capacitance to the flatband potential is also considered.

For this application, the mixer demonstrated that commonplace Si diodes (M/A-COM MA40132) can perform well to temperatures at least as low as 50 K. Although the device used in this study was operated near the theoretical onset of carrier freeze-out, high performance was obtained. A possible advantage of Si over GaAs for this particular application is lower barrier height, which allows use of a smaller LO drive level, perhaps thereby eliminating the need for dc bias. The minimum practical barrier height obtainable for a metal/*n*-type GaAs Schottky contact is about 0.75 eV, whereas barrier heights of less than 0.5 eV can be produced on *n*-type Si.

Symbols

A^*	Richardson constant
C_j	junction capacitance
C_{j0}	zero bias junction capacitance
$C_j(v_j(t))$	time varying junction capacitance
$C_{j\max}$	maximum junction capacitance
C_n	Fourier coefficients of periodic junction capacitance
C_p	package capacitance
E_c	conduction band energy level
E_d	energy level of weakly bound donor sites
E_g	bandgap energy
f_{LO}	local oscillator frequency
f_{RF}	signal frequency
$g_{0,1,2}$	conductance waveform Fourier coefficients
I-V	current-voltage
$I_{m,n}$	m and nth order modified Bessel functions
I_r	rectified current
I_s	saturation current
i_{IF}, i_{IM}, i_{RF}	intermediate, image, and signal frequency currents
i_{om}	total diode direct current for a modified "Y-mixer"
i_{oy}	direct current for a pure "Y-mixer"
k	Boltzmann's constant
L	feed line attenuation
$L_{I,O}$	input, output feed line loss
L_M	mixer conversion loss
L_p	lead beam inductance
l	incremental feed line loss
N	number of infinitesimal matched lossy lines
N_D	donor concentration
N_D^+	number of ionized donor sites
q	electron charge
R_j	junction resistance
R_s	diode series resistance
S	junction area
T	temperature
$T_{I,O}$	input, output feed line noise temperature
T_M	mixer noise temperature
T_P	estimated average of physical temperatures at ends of feed lines
T_{SYS}	measured system noise temperature
T'	reduced temperature
t	time
V_{DC}	bias voltage
V_f	diode forward bias
V_j	junction voltage
$V_{j1,2}$	fundamental, second harmonic junction voltage
$V_{LO} + V_{DC}$	peak instantaneous voltage
v_{IF}, v_{IM}, v_{RF}	intermediate, image, and radiofrequency voltages
α	$q/\eta kT$
Γ	source or load reflection coefficient
δ	$\frac{g_1^2}{g_0^2 - g_1^2} \cdot \frac{g_0 - g_2}{g_0 + g_2}$ for an open circuit; $\frac{g_1^2}{g_0^2}$ for a short circuit
η	ideality factor
η'	ideality factor at reduced temperature
ϕ_b	barrier height
ϕ_{bi}	flatband potential
ω	radian frequency

Acronyms:

HEMT	high electron mobility transistor
IF	intermediate frequency
LO	local oscillator
RF	radiofrequency
S-parameter	scattering matrix
SSB	single sideband
VSWR	voltage standing wave ratio

Device Model

A precise equivalent circuit representing the diode, as well as an accurate description of its band structure, was required if the mixer design was to be optimized. Harmonic balance techniques could then be used to determine junction conductance and capacitance waveforms, and conversion characteristics could be estimated. It is well known that the *I–V* characteristic, particularly the ideality factor η and the barrier height ϕ_b, are strongly influenced by operating temperature. Diode current becomes much more sensitive to voltage at cryogenic temperatures, as indicated by the thermionic emission equation. Consequently, the slope of the *I–V* curve becomes steeper, and the knee occurs at higher voltages. The measured *I–V* curves for this particular low barrier Si diode are shown in figure 2. Since minimizing conversion loss means maximizing junction conductance variation, achieving good performance requires greater LO power or dc bias. In addition to counteracting the effect of cooling, dc bias can be used to control the average value of the diode's conductance waveform, thereby providing a method to control impedance.

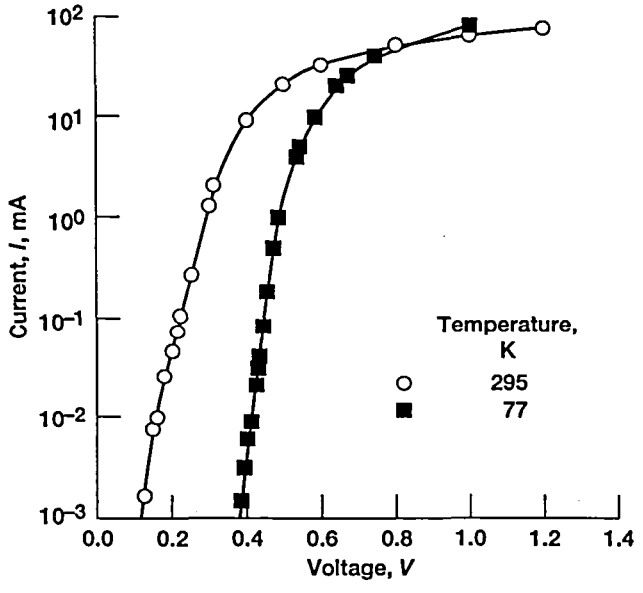

Figure 2.—Measured *I-V* curves for Si diode at 77 and 295 K.

The Si diodes used in this application were arsenic doped with a donor concentration of $N_D = 1.2\times10^{17}/\text{cm}^3$. There may be a significant tunneling current component for this doping density at the specified operating temperature (ref. 8). For the purpose of modeling the diode, it was assumed that this effect could be adequately accounted for by using the measured ϕ_b and η in the pure thermionic emission equation given in equation (2).

At room temperature, Si has a bandgap (E_g) of 1.12 eV (the bandgaps of most semiconductors have a negative temperature coefficient). At 77 K the calculated bandgap of Si is 1.166 eV (ref. 9). The slight reduction in the bandgap resulting from the reduced pressure in the cryostat (~10 mtorr) is of negligible consequence insofar as the model is concerned. It can also be shown that at 77 K the carrier concentration equals the number of ionized donor sites N_D^+, and band-to-band excitation is negligible. Excitation to the conduction band E_c occurs only from weakly bound donor sites (E_d), which reside at about 0.054 eV below E_c. From the closed form expression of the Fermi-Derac integral, N_D^+ can readily be estimated as $8.6\times10^{15}/\text{cm}^3$ if the semiconductor is assumed to be nondegenerate. The Fermi level is in fact about 6 kT/q from the conduction band edge. The barrier height was calculated from the modified saturation current expression proposed by Bhuiyan et al (ref. 10). Zero bias barrier height is expressed as the product of the temperature-dependent ideality factor η and the apparent barrier height obtained from the diode *I–V* characteristic. It was calculated to be equal to 0.570 V from

$$\phi_b = \frac{1}{\alpha}\cdot\ln\left(\frac{A^*\cdot S\cdot T^2}{I_s}\right) \qquad (1)$$

where $\alpha = q/(\eta kT)$; A^* is the Richardson constant; S is the junction area; k is the Boltzmann constant; and q is the electron charge. The calculated value is the thermal equilibrium value. Under forward bias, the barrier height would be slightly higher because of the Schottky effect; hence, the calculated value is, in this sense, conservative. An error of two within the natural log term introduces an error of only about kT/q to the calculation. Flatband potential ϕ_{bi} is the difference between the barrier height and the difference in potential between the Fermi level and the conduction band; it was calculated to be 0.529 V (ref. 9). The measured value of η at 77 K, as obtained directly from the *I-V* characteristic, was 2.3 compared to a room temperature value of 1.3. Saturation current I_s was calculated by fitting the thermionic emission equation (eq. 2) to the linear portion of figure 2. Its calculated value was 1.9×10^{-17} A, as opposed to 4.3×10^{-8} A at room temperature. Figure 3(a) shows the Schottky barrier energy band diagram based on these calculations.

For $I >> I_s$ the equation governing the forward *I–V* characteristic is

$$I \approx A^*\cdot S\cdot T^2\cdot e^{\alpha\cdot(V_f-\phi_b-I\cdot R_s)} \qquad (2)$$

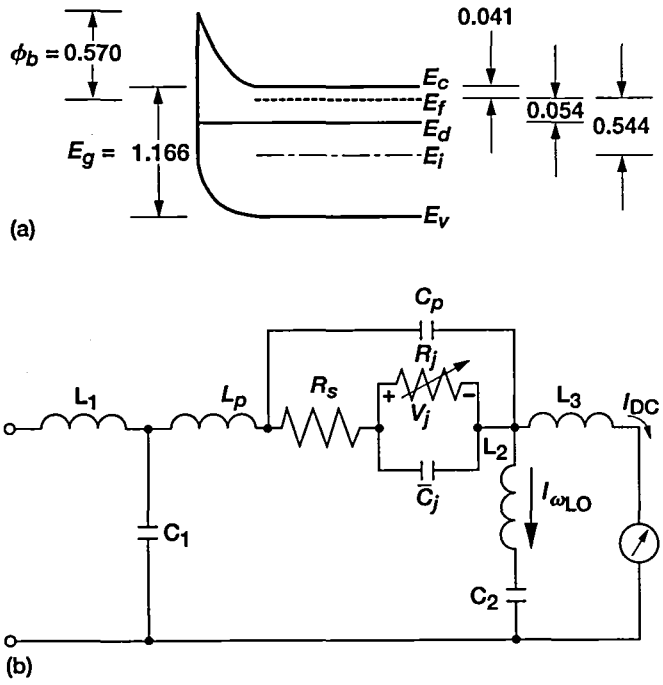

Figure 3.—Schottky junction energy band diagram at 77 K. (a) Calculated in electron volts, no scale. (b) Diode equivalent circuit with embedding schematic (L_1, C_1, L_2, and C_2 are frequency-dependent and represent matching circuit (subscript 1) and radial stub (subscript 2); L_3 is wire bond).

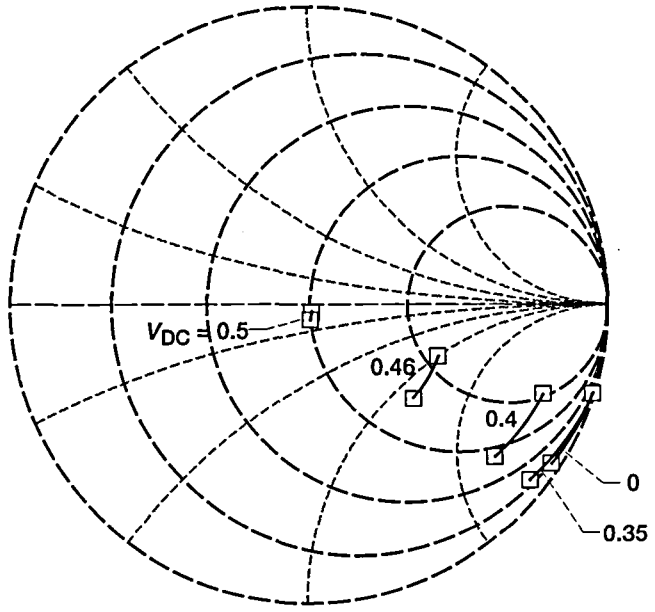

Figure 4.—De-embedded diode impedance data at 77 K as a function of dc bias with -20 dBm RF drive (RF = 5.0 to 10.0 GHz).

where ϕ_b and η, incorporated into α, are implicitly taken to be functions of temperature, and V_f is the forward bias, and R_s the diode series resistance.

The quasi-static circuit model shown in figure 3(b) consists of the voltage-controlled junction resistance (R_j) and junction capacitance (C_j); a fixed series resistance; package capacitance (C_p); and beam lead inductance (L_p). The value of R_s was obtained by plotting the difference between the voltage from the measured log I–V curve and that from the closest fitting straight line projected from the linear region at several high current levels. The slope of the resulting straight line yielded an R_s of 5.7 Ω, which was essentially independent of temperature. The device impedance was measured at 77 K with a network analyzer coaxially coupled to the diode, which was bonded to a coplanar waveguide carrier mounted in a closed-cycle He refrigerator. Calibration established the reference plane at the carrier input terminal, and the electrical path length from the measurement plane was subtracted. De-embedded impedance data are shown in figure 4. With no dc voltage applied, the parasitic reactances and the zero bias junction capacitance C_{j0} were determined by tickling the diode with a –20 dBm signal. The forward voltage was then incrementally adjusted up to flatband. Even though a narrow band match was desired, a broadband sweep was used to improve the modeling accuracy. The model's intrinsic parameters were then adjusted to match the measured S-parameters while the parasitic element values were held constant (Lp = 0.022 nH; Cp = 0.020 pF).

Circuit Design

The layout of the mixer is shown in figure 5. A singly balanced topology with a 180° hybrid ring was selected after tradeoffs based on size, power requirements, port-to-port characteristics, and bandwidth were made (ref. 11). The complete circuit on 0.020-in.-thick Al_2O_3 measured 0.8 in.^{2}, as opposed to 1.3 in.^{2} for a comparable single-ended mixer that had previously been designed. Since the mixer was to be operated inside a cryostat, low mass was desirable to facilitate cooldown. The requirement for high LO-to-RF isolation to prevent the possibility of pre-amplifier dynamic range degradation suggested the use of a 180° hybrid instead of a 90° quadrature coupler. A double balanced mixer would have required at least twice the LO power and provided excess bandwidth. The center frequency of the ring was at the LO frequency of 8.3 GHz; hence the diodes were, in principle, pumped 180° out of phase, and spurious rejection was maximized. Quarter-wave radial stubs served as virtual grounds for the diodes at the RF and LO frequencies. These were bypassed to ground through chip capacitors connected by a wire bond to the vertex of the stub for the intermediate frequency (IF) return path. The IF-port low-pass filter was based on a Chebyshev prototype (ref. 12), and its passband and stopband characteristics were fairly insensitive to the input termination over a range of 100 to 150 Ω The filter was designed to present an open circuit at the

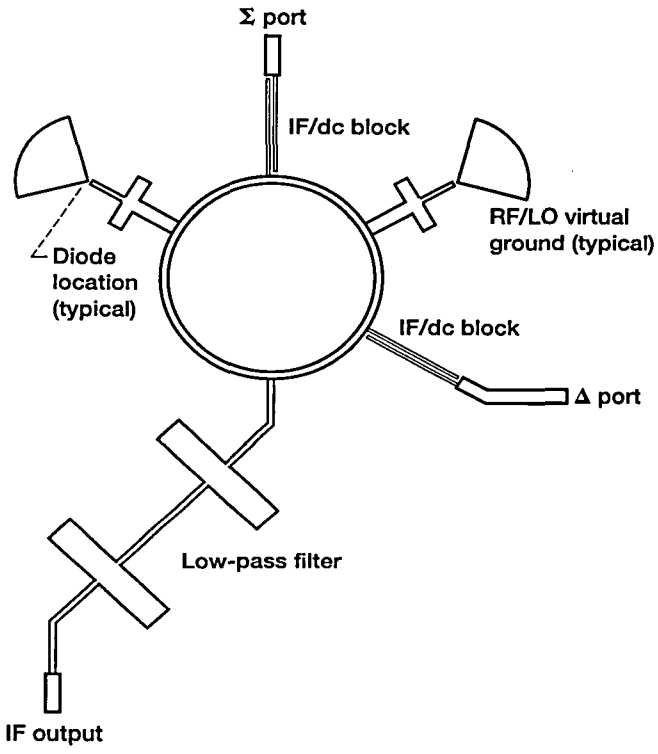

Figure 5.—Layout of matched mixer (circuit is 0.75 in. wide and 0.98 in. long).

LO frequency and did in fact provide greater than 30 dB attenuation to all spurious responses between 6 and 18 GHz. Quarter-wave coupled parallel lines at the RF and LO ports acted as dc and IF blocks. Both the low-pass filter and the dc and IF blocks were evaluated separately from the mixer. The matching circuit was extended past the ring by a 50 Ω line to minimize electromagnetic interaction between adjacent microstrip structures.

Harmonic balance techniques (ref. 13) were used to design an embedding impedance network starting from a conventional stub-tuned signal conjugate matching circuit. Since the intermediate frequency was relatively low, the circuit also provided a reasonable match to the LO over a limited pump range. Inherent low-pass characteristics of the matching circuit and the impedance periodicity of the radial stubs were tailored to present purely reactive terminations at the second and third LO harmonics. This resulted in a reasonably good open circuit at the sum. If we assume that the alternate diode port can be represented by the simple model of figure 3(b), the concept can be illustrated by figure 6, which shows the diode embedding "impedance." Johnson (ref. 14) showed that an open circuit image termination provides minimum conversion loss in the case of a sinusoidal constant-voltage-source LO. The admittance at the image frequency was 0.0017 - j0.0043 mhos. Note that the matching and termination strategy employed here does not readily lend itself to a situation in which the image is below the signal frequency.

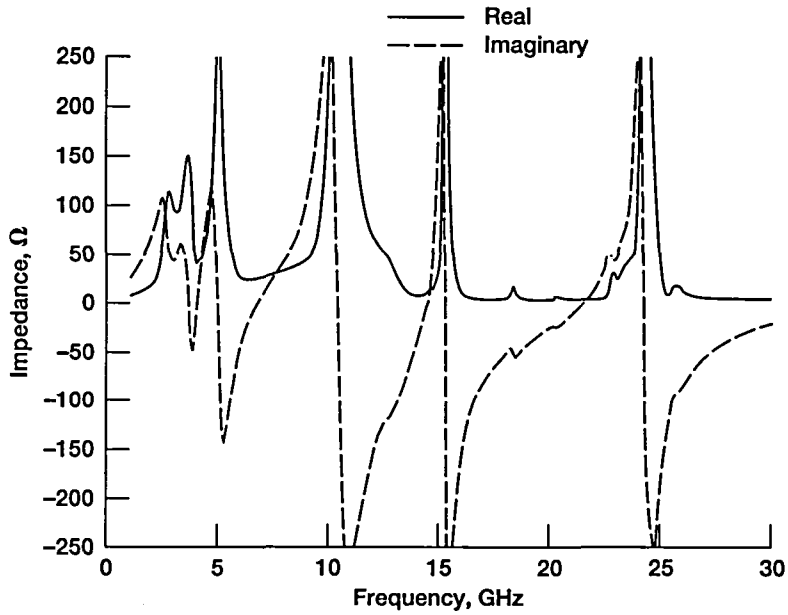

Figure 6.—Real and imaginary part of diode embedding impedance.

Junction Capacitance and Flatband

Crowe and Mattauch (refs. 6 and 7) have argued that mixer diodes must be pumped beyond flatband if minimum conversion loss is to be obtained. Despite the increase in junction capacitance that occurs near flatband, according to the usual analytical expression for an abrupt junction

$$C_j(V_j) = \frac{C_{j0}}{\sqrt{1 - \frac{V_j}{\phi_{bi}}}} \qquad (3)$$

diode conductance only then is allowed to swing over its maximum value. It is generally accepted that conversion loss is minimized only when the junction conductance variation is permitted to include the junction conductance extremes. (To a first order from the simple model of fig. 3(b), the minimum diode conductance is approximately $R_s(\omega C_j)^2$, and the maximum is R_s^{-1}.) The capacitance expressed in equation (3) is based on an approximation that deteriorates as forward voltage approaches the flatband, yet it is widely used in mixer analysis. The average value can be calculated from equation (3) as

$$\bar{C}_j = \frac{1}{\phi_{bi}} \lim_{\varepsilon \to 0} \int_0^{\phi_{bi} - \varepsilon} C_j(V_j)\, dV \qquad (4)$$

The foregoing improper integral is convergent, and the mean value becomes $2C_{j0}$. This, however, is too large a value to assume for the average $C_j(V_j(t))$ (which can be partially tuned out). A more exact numerical analysis, indicating a much less dynamic change in C_j near flatband, was reported by Siegel et al. (ref. 15). The modeled data extracted from the experiment reported herein and presented in figure 7 support their theoretical work. A zero bias junction capacitance of 0.077 pF was obtained, with a mean value of about 0.085 pF. Although it is conceivable that there is some excursion between the fourth and fifth data points, the salient features are that the capacitance increases more slowly than predicted and that $C_{j\max}$ occurs in advance of the flatband potential. The time varying capacitance waveform $C_j(V_j(t))$ was calculated based on the data of figure 7 and contrasted to equation (3). The results, shown in figure 8, correspond to a +1 dBm sinusoidal LO drive and a dc bias of 0.424 V. The average components are 0.098 and 1.771 pF for the experimental and analytical data, respectively. For the various bias and LO drive conditions tested ($0.55\ \phi_{bi} < V_{DC} < 0.85\ \phi_{bi}$), the time average capacitance was always within 20 percent of the mean value extracted from figure 7. Still, for design (i.e., matching) purposes, the average component of the time varying capacitance should be used.

There is an intricate relationship between junction capacitance, flatband potential, and conversion loss. Since minimizing conversion loss requires maximizing junction conductance

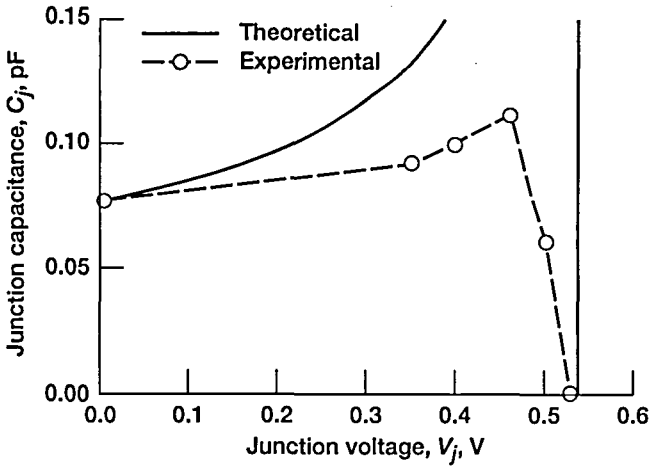

Figure 7.—Junction capacitance derived from RF measurements and theoretical curve from analytic expression (eq. 3).

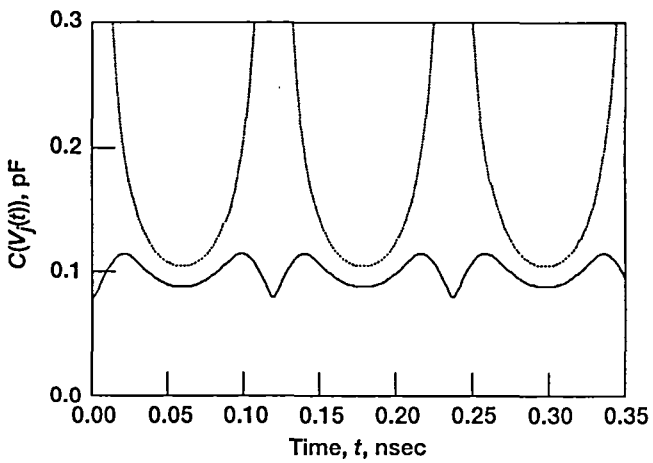

Figure 8.—Time varying capacitance waveform based on experimental data (solid line) and analytical expression (dashed line). Maximum capacitance derived from equation (3) was arbitrarily truncated at 10 C_{j0}.

variation, it is natural to expect that the LO drive must exceed the value corresponding to a situation in which the diode current exceeds the flatband current. However, excess LO drive causes an increase in overall loss because of dissipation in R_s. Moreover, at points beyond the point where the junction resistance is limited by R_s, an increase in the LO drive simply increases the effective pulse duty ratio, which reduces the relative conversion conductance (refs. 16 and 17). Crowe and Mattauch (refs. 6 and 7) showed that minimum loss is obtained only when the peak instantaneous voltage ($V_{LO} + V_{DC}$) **exceeds** the flatband voltage. Their numerical model assumed that there was a sinusoidal LO voltage across the diode terminals and that higher order sidebands and LO harmonics were short circuited. This arrangement is commonly referred to as a "Y-type" mixer,

after Saleh (ref. 18), since the only way to determine the currents (i_{RF},i_{IM}, and i_{IF}) as explicit functions of the signal, image, and intermediate frequency voltages (v_{RF},v_{IM}, and v_{IF}) is to use a *Y*-matrix representation of the time-dependent junction conductance. The analysis presented herein determined diode voltage from measurement of the rectified current (I_r) and knowledge of the diode terminations up to three LO harmonics. (The voltage drop across R_s was not negligible and was subtracted from the applied bias to determine junction voltage. Bias supply leads contributed only 0.13 Ω/ft and were ignored.) Saleh (ref. 18) derived an expression for rectified current in the case of an exponential diode *Y*-mixer with an open circuited second harmonic. However, his approximation is valid only for large pump voltages, that is, for $V_j >> \eta(kT/q)$. The analysis that follows can be used to show that the assumption is only marginally satisfied for this mixer at drive levels ≤ 1 dBm. Torrey and Whitmer (ref. 19) developed the general admittance matrix for this modified *Y*-mixer by expanding the current in terms of a double Fourier series. An extension of their approach shows the total diode direct current to be equal to

$$i_{om} = I_s \cdot \left[e^{\alpha V_{DC}} \left(\sum_{n,m} I_n(\alpha V_{j1}) \cdot I_m(\alpha V_{j2}) \right) - 1 \right] \quad (5)$$

over all integers n and m where $n = -2m$ and I_n is the nth order modified Bessel function. The junction voltage of the second harmonic V_{j2} was determined numerically by setting the second harmonic current to zero. Five different bias and pump conditions yielded a mean value of 0.585 V, with a standard deviation of 0.034 V for the total bias voltage, which provided minimum conversion loss in each case. The direct current for a pure *Y*-mixer (ref. 18) is

$$i_{oy} = I_s \cdot e^{(\alpha V_{DC})} \cdot I_0(\alpha V_j) \quad (6)$$

Again, from the same five measurements, a mean value of 0.537 V with a standard deviation of 0.011 V was obtained. The impedances at the second and third LO harmonics were, in fact, purely reactive, so presumably the true voltage lies somewhere in between. This mean value clearly exceeds the voltage at which C_{jmax} occurs, but barely exceeds the flatband voltage.

Experimental Results and Discussion

The mixer was bonded with silver paint to a gold-plated brass fixture. The fixture was bolted to the cold finger of a thermostatically controlled closed-cycle He refrigerator interfaced with semirigid coaxial ports. Indium foil between the fixture and the cold finger ensured good thermal contact. A thermocouple was bolted to the fixture adjacent to the mixer substrate to determine the diode temperature. Power meters with coaxial thermistor mounts measured RF and LO input power at the ports of the cryostat. The voltage standing wave ratio (VSWR) was measured with power meters connected to a 20 dB (± 0.1 dB) coupler that had 44 dB directivity. To determine spurious product power levels, the IF port was connected to a spectrum analyzer through a dc block. The IF signal power was measured with a power meter.

Data to be presented are for source and load impedances of nominally 50 Ω. Table I presents data for mixers with and without matching circuits. The isolation characteristics of this mixer were determined primarily by the hybrid ring coupler, but the VSWR's depend on the impedance of the individual diode ports. With an LO drive of +1 dBm, the matching and enhancement circuitry lessened conversion loss by almost 2 dB. (With an LO drive of 0 dBm, the conversion loss was 3.7 dB.) On the basis of the VSWR improvement, we can attribute 0.5 dB of the enhancement to matching. These results correspond to a situation in which the LO pumps the delta port. The image frequency power appearing at the RF port was no greater than −32 dBm.

TABLE I.—TYPICAL PART CHARACTERISTICS OF MIXERS WITH AND WITHOUT MATCHING CIRCUITS

	Isolation, dB				Voltage standing wave ratio	
	LO to RF	RF to LO	LO to IF	RF to IF	RF	LO
Unmatched	33	18	43	37	2.1	1.6
Matched	36	14	45	37	1.2	1.5

Conversion loss and bias conditions as a function of temperature are shown in figure 9 for both a +1 and +10 dBm LO drive level with f_{RF} = 7.16 GHz. The RF input power was −15.0 dBm. Performance criteria could be met down to at least 50 K by increasing the bias voltage slightly. Typical rectified currents recorded at optimum bias levels at about 77 K were as follows:

Local oscillator power, dBm	Rectified current, I_r, mA
0	2.36
+1	2.63
+10	6.84

The change in current when the RF power was toggled on or off was imperceptible.

The noise figure was obtained by using an HP–8970B noise figure meter and an HP 346A noise source. The physical temperature of the noise source, which was generally above 290 K, was accounted for by the meter. Calibration planes were established

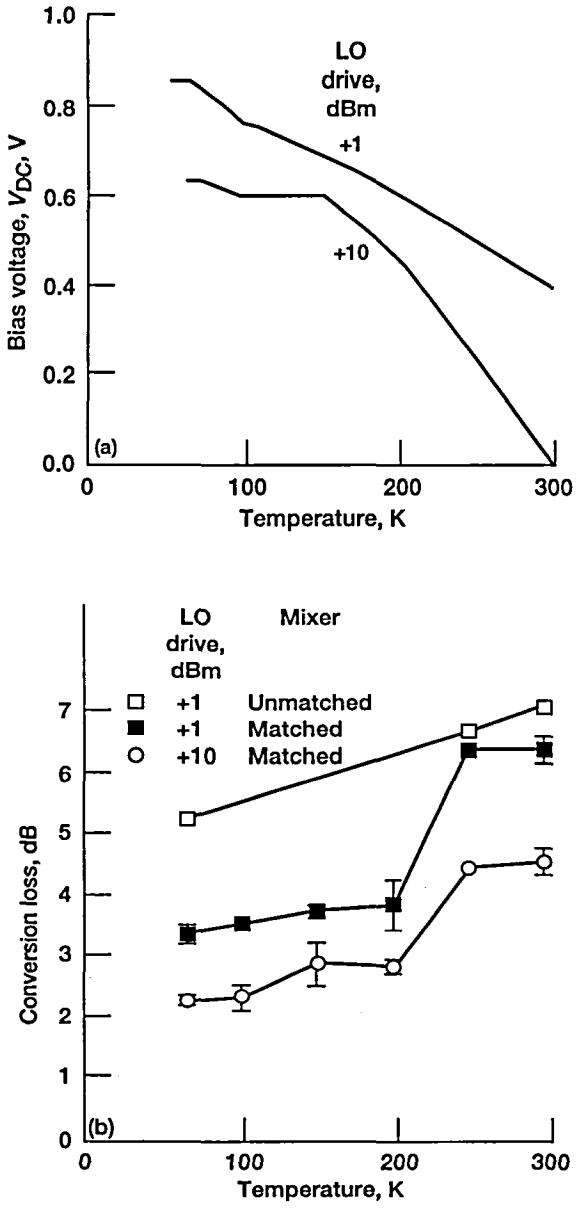

Figure 9.—Typical bias voltage and conversion loss at +1 and +10 dBm LO drive as a function of temperature. (a) Bias voltage. (b) Conversion loss (RF is approximately 7.2 GHz; LO frequency is 8.3 GHz). Error bars represent range of measured data for three different mixers. All diodes were from the same lot.

at the cryostat I/O (input/output) connectors. Impedance mismatches were small ($|\Gamma|^2 << 1$) and, consequently, neglected. Such a decision was justified for the cooled, matched mixer since the RF VSWR was very small. Furthermore, the measured conversion loss agreed exceedingly well with the theoretical conversion loss. (This will be demonstrated in the next section.) This implied that there was not a significant mismatch at the IF port either. In general, mismatch loss cannot be ignored (refs. 20 and 21). (Since noise power must obey all power transfer laws, a mismatch results in only $(1 - |\Gamma|^2)$ of the available power actually being measured. Additionally, a lossy feed line would contribute $|\Gamma|^2$ times the feed noise temperature because of re-reflection from the mismatch.) Mixer noise temperature can be calculated as

$$T_M = T_{SYS}/L_I - T_I/L_I - T_O L_M \tag{7}$$

where T_{SYS} is the measured system noise temperature, L_I is the input feed line loss, and L_M is the mixer conversion loss. Feed line noise temperature $T_{I,O}$ is given by

$$T_{I,O} = (L_{I,O} - 1)\, T_P \tag{8}$$

Here, L_O is the output feed line loss, and T_P is estimated as the average of physical temperature at the ends of the feed lines. For small losses (<1 dB), this assumption introduced negligible error. If a feed line with attenuation L (dB) is regarded as a series of N infinitesimal, matched lossy lines at physical temperature T_n, and if each elemental section has loss l, it can be shown that the equivalent noise temperature is

$$T_e = \sum_{n=1}^{N} l^{n-1} (l - 1)\, T_n \tag{9}$$

Here, T_n is given by

$$T_n = T_0 - \left(\frac{T_0 - T_{N+1}}{N}\right)\left(n - \frac{1}{2}\right) \tag{10}$$

and l is defined

$$l = 10^{L/10N} \tag{11}$$

In the strictest sense, l is not a constant since conductor loss will improve slightly at the cold end of the line. The values T_0 and T_{N+1} are the physical temperatures at the input and output of the feed line, respectively. Equation (9) applies only for a linear temperature gradient. That is, when the ends of the line are in good thermal contact with T_0 and T_{N+1}, thermal equilibrium has been established, and the line has a uniform cross section. For the lines used here, the difference between equation (9) in the limit as $N \to \infty$ and the noise temperature calculated by using T_p is less than 1 K.

A low pass filter with greater than 40 dB of attenuation at the image frequency was placed before the input port. At +1 dBm, the single-sideband (SSB) associated noise figures at 77 and 295 K were 3.7 and 5.1 dB, respectively. At +10 dBm, the corresponding noise figures were 4.3 and 5.4 dB.

Measurement uncertainty was poor, about 1 dB, because of mixer loss and second stage (instrumentation) noise (ref. 22). By using a calculated value of –68 dBm input noise power to the HP–8970B, along with the HP–8970B specifications, the second stage noise figure was determined to be about 10 dB. A low noise pre-amplifier inserted between the IF and the noise meter would, of course, improve the uncertainty considerably.

If the conversion loss of about 2.3 dB with +10 dBm LO drive is dissected into its intrinsic and parasitic parts, it agrees extremely well with the minimum theoretical value. A good approximation of parasitic loss can be obtained by using the equivalent circuit of figure 3(b) and evaluating the ratio of available power to power delivered to the junction resistance (ref. 23) such that

$$L = 10 \cdot \log\left[1 + \frac{R_s}{R_j} + (\omega \cdot \bar{C}_j)^2 \cdot R_j \cdot R_s\right] \qquad (12)$$

The minimum value, 0.16 dB, occurs when $R_j = 1/\omega\bar{C}_j$. The measured insertion loss of the input coupled lines and passband of the IF filter combination was about 0.7 dB. The RF mismatch loss was about 0.05 dB (for this design, the minimum conversion loss occurred at the minimum VSWR). Hence, an upper limit for the intrinsic loss due to finite junction conductance is about 1.39 dB. Actually, it is probably better than this since equation (12) does not include loss at the intermediate frequency, and hybrid loss was neglected.

A lower limit on intrinsic loss can be estimated by expressing the admittance of the junction in standard matrix form (refs. 17 and 19):

$$\begin{bmatrix} i_{RF} \\ i_{IF} \\ i_{IM} \end{bmatrix} = \alpha \cdot I_s \cdot e^{\alpha V_{DC}} \begin{bmatrix} I_0(\alpha V_j) & I_1(\alpha V_j) & I_2(\alpha V_j) \\ I_1(\alpha V_j) & I_0(\alpha V_j) & I_1(\alpha V_j) \\ I_2(\alpha V_j) & I_1(\alpha V_j) & I_0(\alpha V_j) \end{bmatrix} \cdot \begin{bmatrix} v_{RF} \\ v_{IF} \\ v_{IM} \end{bmatrix} \qquad (13)$$

This admittance matrix is real, brazenly ignoring junction capacitance. It is conceded that the capacitance variation is important to mixer analysis (refs. 24 and 25), but the purpose here was to demonstrate how closely this design approximated the performance expected from a nonlinear resistance with a classical exponential characteristic. The matched signal loss for a reactively terminated image becomes

$$L_M = \frac{1 + \sqrt{1-\delta}}{1 - \sqrt{1-\delta}} \qquad (14)$$

where

$$\delta = \frac{g_1^2}{g_0^2 - g_1^2} \cdot \frac{g_0 - g_2}{g_0 + g_2} \qquad (15)$$

and for the open circuited case,

$$g_n = \alpha I_s e^{\alpha V_{DC}} I_n(\alpha V_j) \qquad (16)$$

The theoretical conversion loss is found from equation (14) to be 1.36 dB. Similarly, for a +1 dBm LO drive, theoretical conversion loss is 2.40 dB. For a short circuited image,

$$\delta = \frac{g_1^2}{g_0^2} \qquad (17)$$

It should be noted that for the present mixer, $\omega\bar{C}_j r_s << 1$ and $|\omega C_n| << |g_n|$, where C_n are the Fourier coefficients of the periodic junction capacitance $C_j(V_j(t))$ from figure 8.

The mixer's improvement over its room temperature performance can be attributed, in part, to the deliberate match to the diode characteristics at 77 K. The conductance waveshape and the average junction conductance are directly influenced by temperature. Furthermore, the minimum diode conductance, defined earlier, may be temperature-dependent and could modify the average junction resistance. Moreover, it is well established that both the conversion loss and noise figure are functions of the conductance waveform and embedding impedance, with the conductance waveform generally expressed as a Fourier series as was done in equation (13). The Fourier coefficients (g_n) depend on pump voltage, operating temperature, and bias, and the ratios g_1/g_0 and g_2/g_0 approach unity as loss is minimized. These conductance ratios can approach unity much more rapidly at cryogenic temperatures. That is, a given ratio can be obtained with less LO power because of the enhanced nonlinearity (i.e., the pumped diode more closely resembles an ideal switch). Weinreb and Kerr (ref. 3) showed that to maintain a given conversion loss and impedance level, the LO power should be reduced by $(\eta T/\eta' T')^2$, where the primed symbols correspond to the lower temperature. However, they also showed that the dc bias voltage must increase accordingly, thereby increasing the mean junction capacitance by a factor of $(\eta T/\eta' T')^{1/2}$. Presumably, the total conversion loss will degrade since its lower limit, imposed by junction parasitics, is inversely proportional to the diode cutoff frequency. The experimental work reported herein supports the more recent theoretical analysis of Crowe and Mattauch (refs. 6 and 7), which predicts that loss degradation due to cooling need not occur. Their model assumed that the junction capacitance behaved in the same way regardless of operating temperature.

Summary and Conclusions

The inevitability of degradation in the conversion loss of diode mixers on cryogenic cooling has long been debated. A flight-qualified mixer developed specifically for operation at cryogenic temperatures was demonstrated, and an appreciable reduction in loss was observed. The ordinary Si diodes employed were found to work well for this mixer to at least 50 K, even though other applications of Si junctions can potentially suffer from carrier freeze-out effects. A novel, but straightforward, combination matching and reactive termination circuit was designed to optimize the mixer so as to minimize both loss and pump power. Each diode was separately, but identically, terminated. The negative temperature coefficients of barrier height and ideality factor were incorporated into the design. Clearly, the increased nonlinearity of the cooled diode can be used to an advantage, despite the presumed increase in mean junction capacitance on cooling. There is evidence to suggest that the junction capacitance departed from the monotonic behavior predicted by the usual analytic expression. The results also showed that the minimum conversion loss was obtained when the total bias (V_{LO} + V_{DC}) significantly exceeded the bias at maximum junction capacitance and the flatband voltage by about 5 percent. These foregoing design principles are believed to be important for precision mixers and, especially, for applications such as hybrid superconductor-semiconductor receivers.

Acknowledgments

The author is grateful for the efforts of Charles Hulbert, Elizabeth McQuaid, and Nicholas Varaljay, through whose dedication numerous mixers were fabricated in a short period of time. The author also gratefully acknowledges the contribution of Bruce Viergutz, who provided assistance during the testing and space qualification of these mixers.

Lewis Research Center
National Aeronautics and Space Administration
Cleveland, Ohio, April 13, 1995

References

1. Duh, K.H.G., et al.: 32 GHz Cryogenically Cooled HEMT Low-Noise Amplifiers. IEEE Trans. Electron Devices, vol. 36, no.8, Aug. 1989, pp. 1528–1535.
2. Yang, C.C., et al.: A Cryogenically-Cooled Wide-Band HEMT MMIC Low-Noise Amplifier. IEEE Micro. Guided Wave Lett., vol. 2, no. 2, Feb. 1992, pp. 58–60.
3. Weinreb, S.; and Kerr, A.R.: Cryogenic Cooling of Mixers for Millimeter and Centimeter Wavelengths. IEEE J. Solid-State Circuits, vol. SC-8, no. 1, Feb. 1973, pp. 58–63.
4. Kerr, A.R.: Low-Noise Room-Temperature and Cryogenic Mixers for 80-120 GHz. IEEE Trans. Microwave Theory Tech., vol. MTT–23, Oct. 1975, pp. 781–787.
5. Barner, J.B., et al.: Design and Performance of Low-Noise Hybrid Superconductor/Semiconductor 7.4 GHz Receiver Downconverter. Applied Superconductivity Conference, Boston, MA., Oct., 1994.
6. Crow, T.W.; and Mattauch, R.J.: Conversion Loss in GaAs Schottky-Barrier Mixer Diodes. IEEE Trans. Microwave Theory Tech., vol. MTT–34, July 1986, pp. 753–760.
7. Crow, T.W.; and Mattauch, R.J.: Analysis and Optimization of Millimeter- and Submillimeter-Wavelength Mixer Diodes. IEEE Trans. Microwave Theory Tech., vol. MTT-35, Feb. 1987, pp. 159–168.
8. Schroder, D.K.: Semiconductor Material and Device Characterization. John Wiley and Sons, New York, 1990.
9. Sze, S.M.: Physics of Semiconductor Devices. Second Ed. John Wiley and Sons, New York, 1981.
10. Bhuiyan, A.S.; Martinez, A.; and Esteve, D.: A New Richardson Plot for Non-Ideal Schottky Diodes. Thin Sol. Fi., 161, 1988, pp. 93–100.
11. Maas, S.A.: Microwave Mixers. Artech House, Inc., Dedham, MA., 1986.
12. Porter, J.: Chebyshev Filters with Arbitrary Source and Load Resistances. RF Design, Aug. 1989, pp. 63–68.
13. *Libra*, EEsof, Inc., 5601 Lindero Canyon Rd., Westlake Village, CA.
14. Johnson, K.M.: X-Band Integrated Circuit Mixer with Reactively Terminated Image. IEEE Trans. Microwave Theory Tech., vol. SC-3, June 1968, pp. 50–59.
15. Siegel, P.H.; Mehdi, I.; and East, J.: Improved Millimeter-Wave Mixer Performance Analysis at Cryogenic Temperatures. IEEE Micro. Guided Wave Lett., vol. 1, no. 6, June 1991, pp. 129–131.
16. Barber, M.R.; and Ryder, R.M.: Ultimate Noise Figure and Conversion Loss of the Schottky Barrier Mixer Diode. Int. Micr. Symp. Digest, May 1966, pp. 13–17.
17. Barber, M.R.: Noise Figure and Conversion Loss of the Schottky Barrier Mixer Diode. IEEE Trans. Microwave Theory Tech. vol. MTT–15, no. 11, Nov. 1967, pp. 629–635.
18. Saleh, A.A.M.: Theory of Resistive Mixers. Cambridge MIT Press, 1971.
19. Torrey, H.C.; and Whitmer, C.A.: Crystal Rectifiers. McGraw-Hill Book Co., New York, 1948.
20. Harris, I.A.: Dependence of Receiver Noise-Temperature Measurement on Source Impedance. Elect. Lett., vol. 2, Apr. 1966, pp. 130–131.
21. Otoshi, T.Y.: The Effect of Mismatched Components on Microwave Noise-Temperature Calibrations. IEEE Trans. Micro. Theory Tech., vol. MTT–16, no. 9, Sept. 1968, pp. 675–686.
22. Hewlett-Packard Application Note 57-2: Noise Figure Measurement Accuracy, Nov. 1988, pp. 1–31.
23. Hewlett-Packard Application Note 995: The Schottky Diode Mixer, Feb. 1986, pp. 1–6.
24. Siegel, P.H.; and Kerr, A.R.: The Measured and Computed Performance of a 140-220 GHz Schottky Diode Mixer. IEEE Trans. Microwave Theory Tech., vol. MTT-32, no. 12, Dec. 1984, pp.1579–1590.
25. Siegel, P.H.; and Kerr, A.R.: Computer Analysis of Microwave and Millimeter-Wave Mixers. IEEE Trans. Microwave Theory Tech., vol. MTT–28, no. 3, March 1980, pp. 275–276.

REPORT DOCUMENTATION PAGE

Form Approved
OMB No. 0704-0188

1. AGENCY USE ONLY (*Leave blank*)	2. REPORT DATE	3. REPORT TYPE AND DATES COVERED
	September 1995	Technical Paper

4. TITLE AND SUBTITLE

An X–Band Mixer Engineered for 77 K Operation

5. FUNDING NUMBERS

WU–506–72–1B

6. AUTHOR(S)

Robert R. Romanofsky

7. PERFORMING ORGANIZATION NAME(S) AND ADDRESS(ES)

National Aeronautics and Space Administration
Lewis Research Center
Cleveland, Ohio 44135–3191

8. PERFORMING ORGANIZATION REPORT NUMBER

E–9495

9. SPONSORING/MONITORING AGENCY NAME(S) AND ADDRESS(ES)

National Aeronautics and Space Administration
Washington, D.C. 20546–0001

10. SPONSORING/MONITORING AGENCY REPORT NUMBER

NASA TP–3538

11. SUPPLEMENTARY NOTES

Responsible person, Robert R. Romanofsky, organization code 5630, (216) 433–3507.

12a. DISTRIBUTION/AVAILABILITY STATEMENT

Unclassified - Unlimited
Subject Category 32

This publication is available from the NASA Center for Aerospace Information, (301) 621–0390.

12b. DISTRIBUTION CODE

13. ABSTRACT (*Maximum 200 words*)

An X-band Si-diode singly balanced mixer developed specifically for cryogenic operation is presented. In order to reduce thermal demands on a mechanical cooler, the mixer was designed to operate with a minimum of local oscillator (LO) power. That is, since the LO had to be cooled to reduce phase noise, it was desirable to minimize the LO drive. Novel embedding circuit strategy was responsible for nearly theoretical performance. The signal-matching circuit simultaneously provided a reactive termination to the image, sum, and first, second, and third LO harmonic frequencies. A conversion loss of 3.2 dB at 77 K with an LO drive of +1 dBm was measured. This loss included IF filter, dc block, and hybrid coupler losses. Mixer conversion loss is shown to be consistent with the theoretical performance limit expected from the intrinsic diode. The relationship among junction capacitance, flat-band potential, and conversion loss is examined.

14. SUBJECT TERMS

Mixing circuits; Radio receivers; Cryogenics

15. NUMBER OF PAGES

13

16. PRICE CODE

A03

17. SECURITY CLASSIFICATION OF REPORT	18. SECURITY CLASSIFICATION OF THIS PAGE	19. SECURITY CLASSIFICATION OF ABSTRACT	20. LIMITATION OF ABSTRACT
Unclassified	Unclassified	Unclassified	